A multilayer approach and its application in modeling QGNSea V1.0: a local gravmetric quasi-geoid model over the North Sea

Yihao Wu [1, 2], **Zhicai Luo** [3], **Bo Zhong**[4], **Chuang Xu**[2, 5]

[1] Key Laboratory of Virtual Geographic Environment, Ministry of Education, Nanjing Normal University, Nanjing, China

[2] State Key Laboratory of Geodesy and Earth's Dynamics, Institute of Geodesy and Geophysics, Chinese Academy of Sciences, Wuhan, China

[3] MOE Key Laboratory of Fundamental Physical Quantities Measurement, School of Physics, Huazhong University of Science and Technology, Wuhan, China

[4]School of Geodesy and Geomatics, Wuhan University, Wuhan, China

[5]School of Civil and Transportation Engineering, Guangdong University of Technology, Guangdong, China

Correspondence to: Yihao Wu (yihaowu@hust.edu.cn) and Chuang Xu (chuangxu@hust.edu.cn)

Abstract: A multilayer approach is set up for local gravity field recovery in the framework of multi-resolution representation, where the gravity field is parameterized as the superposition of the multiply layers of Poisson wavelets located at the different depths beneath the topography. Different layers are designed to recover the signals at various levels, where the shallow and deep layers mainly capture the short- and long-wavelength signals, respectively. The depths of these layers beneath the topography are linked to the locations that different anomaly sources locate, estimated by the wavelet decomposition and power spectrum analysis. For testing the performance of this approach, a gravimetric quasi-geoid over the North Sea in Europe called QGNSea V1.0 is computed and compared with other existing models. The results show that the multilayer approach fits the gravity data better than the traditionally used single-layer one, especially in regions with topographical variation. A Akaike information criterion (AIC) test demonstrates that the multilayer model gives a smaller AIC value, reaches a better balance between the goodness of fit of data and the simplicity of the model. Moreover, the evaluation with independent GPS/leveling data tests the ability of realistic extrapolation of regional models computed from different approaches, showing that the accuracies of QGNSea V1.0 modeled from the multilayer approach are improved by 0.4 cm, 0.9 cm and 1.1 cm in the Netherlands, Belgium and parts of Germany, respectively, compared to the solution computed from the single-layer approach. Further validation with existing models shows QGNSea V1.0 has the best quality, which may be beneficial for studying the ocean circulation between the North Sea and its neighbouring waters.

1. Introduction

Knowing of earth's gravity field at regional scales is crucial for a variety of applications in geodesy. It not only facilitates the use of Global Satellite Navigation System to determine orthometric/normal heights in geodesy and surveying engineering, but also plays a fundamental role in in oceanography and geophysics.

Regional gravity field determination is typically implemented within a framework of remove-compute-restore methodology (RCR) (Sjöberg, 2005), where the long-wavelength signals are often recovered by satellite-only global geopotential models (GGMs) derived from the dedicated satellite gravity missions, such as the GRACE (Gravity Field and Climate Experiment) (Tapley et al., 2004) and GOCE (Gravity Field and Steady-State Ocean Circulation Explorer) (Rummel et al., 2002). Middle- and short-wavelength signals are extracted from the locally distributed gravity-related measurements (Wang et al., 2012; Wu et al., 2017c). Spherical radial basis functions (SRBFs) are of great interest for gravity field modeling at regional scales over years (Eicker et al., 2013; Naeimi et al., 2015). Typically, the widely-used SRBFs method is implemented by the so-called single-layer approach, i.e., the parameterization of gravity field is only based on a single-layer of SRBFs' grid (Wittwer, 2009; Bentel et al., 2013; Slobbe, 2013; Wu et al., 2017c).

It has been suspected for long that if the single-layer approach can extract the full information of local gravity data, and the multi-resolution representation (MRR) method with SRBFs has been investigated over the recent years (Freeden et al., 1998; Fengler et al., 2004, 2007). Freeden and Schreiner (2006) proposed a multi-scale approach based on the locally supported wavelets for determining the regional geoid undulations from the deflections of the vertical. Freeden et al. (2009) demonstrated that the multi-scale approach using spherical wavelets provided local fine-structured features such as those caused by plumes, which allowed a scale- and space-dependent characterization of this geophysical phenomenon. Schmidt et al. (2005, 2006, 2007) developed a multi-representation method for static and spatiotemporal gravity field modeling through SRBFs, where the input gravity signals were decomposed into a certain number of frequency-dependent detail signals, and concluded that this approach could improve the spanning fixed time intervals with respect to the usual time-variable gravity fields. Chambodut et al. (2005) set up a multi-scale method for magnetic and gravity field recovery using Poisson wavelets, and created a set of hierarchical meshes associated with the wavelets at different scales, where a level of subdivision corresponded to a given wavelet scale.

Panet et al. (2011) extended the approach developed by Chamboudt et al. (2005), and applied a domain decomposition approach to define the hierarchical subdomains of wavelets at different scales, which allowed to split a large problem into smaller ones. These results show the multi-scale approach with SRBFs has a good prospective in gravity field recovery, however, to our knowledge, no direct comparisons have been made between the single-layer approach and multi-scale one regarding the performances in local gravity field recovery. Besides, the existing multi-scale methods mainly construct the multi-scale framework in a mathematical sense, where no explicit geophysical meanings are investigated. In this study, inspired by the power spectral analysis of local gravity signals, we develop a new parameterization of SRBFs network in the framework of the MRR idea, i.e., the so-called multilayer approach; and the multiply layers are linked to the anomaly sources at different depths beneath the topography, which aim at recovering the signals at different levels. In this way, the parameterization of multi-scale method can be linked to the different anomaly sources at different depths. Moreover, the performances of the multilayer approach and traditionally-used single-layer one are directly compared in this study, where the advantages and disadvantages of different methods are analyzed.

The structure of the manuscript is as follows: the data in a study area in Europe are firstly described in Section 2. Then, the multilayer approach based on the MRR representation is introduced, and the wavelet decomposition and power spectrum analysis are applied for constructing the networks of Poisson wavelets with the multilayer approach. In addition, the function model based on the multilayer approach is set up, and the method for unknown coefficients of Poisson wavelets is introduced. We construct the multilayer model in section 3, and compare the performances of different approaches. Finally, the gravimetric quasi-geoid over the North Sea called QGNSea V1.0 is modeled by the multilayer approach and compared with other models for cross validations. We summarize the main summaries and conclusions of this study in section 4.

2. Data and method

2.1. Study area and data

A local region in Europe is chosen as a case study, which covers an area of 49 ℃N-61 ℃N latitude and -6 ℃E-10 ℃E longitude, including the mainland of the Netherlands, Belgium, and parts of the North Sea, UK, Germany and France. Point-wise terrestrial and shipborne gravity anomalies are incorporated for testing the approach we developed in this study, which were provided by different institutions, see Slobbe et al. (2014). The details for data pre-processing

procedures can be referred to Wu et al. (2017c), where crossover adjustment and low-pass filter were applied to remove systematic errors and reduce high-frequency noise, respectively, and datum transformations were performed on all the data. Moreover, the satellite-only reference model called GOCO05s with a full degree and order (d/o) of 280 (Mayer-Gürr et al., 2015) and RTM corrections were removed from the original observations to decrease the signal correlation length and smooth the data within the framework of remove-compute-restore (RCR) framework. The details for the RTM reduction and residual gravity data can be found in Wu et al. (2017c).

2.2. Multilayer approach

According to Schmidt et al. (2006, 2007), the multi-resolution representation (MRR) of the Earth's potential $T(\boldsymbol{z})$ on position $\boldsymbol{z}$ is expressed as

$$T(\boldsymbol{z}) = \bar{T}(\boldsymbol{z}) + \sum_{i=1}^{I} t_i(\boldsymbol{z}) + \delta(\boldsymbol{z}) \tag{1}$$

where $T(\boldsymbol{z})$ is the disturbing potential in this study, $\bar{T}(\boldsymbol{z})$ means a reference model, e.g., a global geopotential model (GGM) computed from spherical harmonics; $\delta(\boldsymbol{z})$ represents the unmodeled signals; I is the number of levels (resolutions); $t_i(\boldsymbol{z})$ is the detailed signal of level i, and the higher the level value i is, the finer are the structures extractable from the input data; $t_i(\boldsymbol{z})$ is computed as the a linear combination of SRBFs (Schmidt et al., 2007)

$$t_i(\boldsymbol{z}) = \sum_{k=1}^{K_i} \beta_{i,k} \Psi_i(\boldsymbol{z}, \boldsymbol{y}_{i,k}) \tag{2}$$

where $\Psi(\boldsymbol{z}, \boldsymbol{y})$ is the SRBF, K_i and $\beta_{i,k}$ are the number and unknown coefficient of SRBF at level i, respectively, and $\boldsymbol{y}_{i,k}$ is the position of SRBF at this level.

We work with the RCR technique, and the reference GGM and RTM corrections are removed from the original data to decrease the signal correlation length and smooth the data (Omang and Forsberg, 2000). Then, only the residual gravity potential $T_{res}(\boldsymbol{z})$ is parameterized by SRBFs using the MRR approach. Neglecting the unmodeled signals, the residual

potential is expressed as a series of the detailed signals at different levels when combining Eq.(1) and Eq.(2)

$$T_{res}\left(\boldsymbol{z}\right)=\sum_{i=1}^{I}\sum_{k=1}^{K_i}\beta_{i,k}\Psi_i\left(\boldsymbol{z},\boldsymbol{y}_{i,k}\right) \tag{3}$$

where Ψ_i is computed as the difference of the spherical scaling functions with low-pass filter characteristics between the consecutive levels $i+1$ and i, but also can be expressed as the SRBF has the band-limited properties in the frequency domain (Schmidt et al., 2007). In this study, Ψ is chosen as the Poisson wavelet with band-limited properties (Chambodut et al., 2005), and its full definition can be found in Holschneider and Iglewska-Nowak (2007).

Poisson wavelets can also be identified as the multipoles inside the Earth, and the scales of Poisson wavelets can be linked to their depths, which are the key issues that determine their properties in space and frequency domain (Chambodut et al., 2005). The detailed signal at level i in Eq.(2) can be estimated by a linear combination of Poisson wavelets located at a specific depth. Poisson wavelets at depths demonstrate different properties in the frequency domain, as the depths going shallower, the scales decrease, and their spectrums shift towards the high degrees of the spherical harmonics (SH) and become more sensitive to the local features of signals with high-frequency properties, and vice versa (Chambodut et al., 2005). These properties are crucial for local gravity field modeling. First, the residual disturbing potential is typically the band-limited signal within the RCR framework, and Poisson wavelets with band-pass filter characteristics are preferable for band-limited signal recovery (Bentel et al., 2013). Moreover, Poisson wavelets at different depths can be linked to the detailed signals at various levels, which are sensitive to different spectral contents of input signals, and can be used for multi-resolution representation.

Rather than using the name of MRR, we interpret Eq.(3) as the multilayer approach considering Poisson wavelets at different depths have various characteristics, and the different layers are corresponding to the Poisson wavelets' grids at various depths. We place Poisson wavelets on the Fibonacci grids under the topography, and keep these grids parallel with the topography (Tenzer et al., 2012). Instead of associating the Poisson wavelets at different depths to the hierarchical meshes with various levels (Chambodut et al., 2005), we apply a wavelet analysis approach to estimate the depths of multiply layers, inspired by the power spectrum analysis of the residual gravity field. The power spectrum analysis of local gravity signals show the gravity signals are the superposition of the contributions generated from the anomaly sources at different depths; and the signals originated from different anomaly sources have heterogeneous

spectral contents (Spector and Grant, 1970; Syberg, 1972; Xu et al, 2018). Since Poisson wavelets at different depths are sensitive to signals with heterogeneous frequency characteristics, we put Poisson wavelets' grids at the locations where the anomaly sources situate. In this manner, the contributions from the anomaly sources at various depths can be estimated by different layers.

In order to separate the contributions stemmed from different anomaly sources, the wavelet multi-scale analysis, which is an excellent approach to extract the signals at different scales, is applied to decompose the gravity data Δg into wavelet approximation A_W and a number of wavelet details D_w $(w = 1, 2, 3, \cdots, W)$ at different scales (Jiang et al., 2012; Audet, 2013; Xu et al., 2017)

$$\Delta g = A_W + \sum_{w=1}^{W} D_w \tag{4}$$

where W is the maximum order for decomposition, A_W is the regional anomaly caused by deep and large-scale geological bodies, and D_w is the local anomaly originated from shallow and small-scale heterogeneous substances. Wavelets analysis generates low-order wavelet details that are invariant with the decomposition order, and only the high-order wavelet details and corresponding wavelet approximation change with the decomposition order. Based on this property, we can choose the proper decomposition order to derive the desirable solutions.

The decomposed signals reveal the features of geological bodies, the average depths of which can be estimated from the power spectral analysis (Spector and Grant, 1970; Syberg, 1972; Cianciara and Marcak, 1976; Xu et al., 2018)

$$h_w = \frac{1}{4\pi} \frac{\Delta \ln P_k^{\,w}}{\Delta k_w} \quad w = 1, 2, \cdots, W \tag{5}$$

where h_w is the average depth of anomaly source corresponding to wavelet detail D_w; $\ln P_k^{\,w}$ is the logarithmic power spectrum of D_w; $\Delta \ln P_k^{\,w}$ and Δk_w are the change rates for $\ln P_k^{\,w}$ and radial wave number k_w, respectively.

In this study, terrestrial and shipborne gravity anomalies are merged for modeling. Gravity anomalies Δg and quasi-geoid height ζ are related to the disturbing potential based on the multilayer approach as follows:

$$\begin{aligned}\Delta g(\boldsymbol{z}) &\approx -\frac{2}{|\boldsymbol{z}|}T_{res}(\boldsymbol{z}) - \frac{\partial T_{res}(\boldsymbol{z})}{\partial |\boldsymbol{z}|} \\ &= \sum_{i=1}^{I}\sum_{k=1}^{K_i}\beta_{i,k}\left(-\frac{\partial}{\partial |\boldsymbol{z}|}\Psi_i(\boldsymbol{z},\boldsymbol{y}_{i,k}) - \frac{2}{|\boldsymbol{z}|}\Psi_i(\boldsymbol{z},\boldsymbol{y}_{i,k})\right) \\ \zeta(\boldsymbol{z}) &= \frac{T_{res}(\boldsymbol{z})}{\gamma(\boldsymbol{z})} = \sum_{i=1}^{I}\sum_{k=1}^{K_i}\beta_{i,k}\frac{\Psi_i(\boldsymbol{z},\boldsymbol{y}_{i,k})}{\gamma(\boldsymbol{z})}\end{aligned} \tag{6}$$

where γ is the normal gravity value.

We suppose the observational errors are white noises with zero mean, and the gravity field model using the multilayer approach is written as the standard Gauss-Markov model

$$\boldsymbol{l}_j - \boldsymbol{e}_j = \boldsymbol{A}_j\boldsymbol{x},\ E\{\boldsymbol{e}_j\} = 0,\ \mathrm{D}\{\boldsymbol{e}_j\} = \boldsymbol{C}_j = \sigma_j^2\boldsymbol{Q}_j = \sigma_j^2\boldsymbol{P}_j^{-1},\ \ j = 1,2,\cdots,J \tag{7}$$

where $\boldsymbol{x}$ is the $K\times 1$ vector of unknown coefficients, including the unknown parameters of Poisson wavelets of all the layers, i.e., $\boldsymbol{x} = \left[\beta_{1,1},\beta_{1,2},\cdots,\beta_{1,K_1},\beta_{2,1},\beta_{2,2},\cdots,\beta_{2,K_2},\cdots,\beta_{I,1},\beta_{I,2},\cdots,\beta_{I,K_I}\right]'$, and $K = K_1 + K_2 + \cdots + K_I$; $\boldsymbol{A}_j$ is the $m_j\times K$ design matrix of group j, $\boldsymbol{l}_j$ is the $m_j\times 1$ corresponding observation vector, $\boldsymbol{e}_j$ is the $m_j\times 1$ vector of corresponding stochastic errors, m_j is the number of observations in group j, and J is the number of observation groups. $E\{\cdot\}$ and $D\{\cdot\}$ are the expectation and dispersion operators, respectively. $\boldsymbol{C}_j$ is the error variance-covariance matrix of group j, and σ_j^2, $\boldsymbol{Q}_j$ and $\boldsymbol{P}_j$ are the variance factor, cofactor matrix, and weight matrix of group j, respectively.

Data in different groups are assumed to be independent, and the weight matrix $\boldsymbol{P}_j$ is supposed to be the scaled diagonal matrix with white noise properties since it is usually difficult to acquire the realistic full error variance-covariance

matrix in real-life measurements. Point-wise data can be directly combined for modeling through the functional described above. However, the heterogeneous characteristics of the data, in terms of spatial coverages and noise properties, may result in an ill-conditioned normal matrix (Panet et al., 2011). We apply the first-order Tikhonov regularization for tackling the ill-conditioned problem (Kusche and Klees, 2002; Wu et al., 2017a). For a given α (regularization parameter) and κ (regularization matrix), the least-squares solution of Eq.(7) is (Klees et al., 2008):

$$\hat{\boldsymbol{x}} = \left(\sum_{j=1}^{J} \left(\frac{1}{\sigma_j^2} \boldsymbol{A}_j^T \boldsymbol{P}_j \boldsymbol{A}_j \right) + \alpha\kappa \right)^{-1} \left(\sum_{j=1}^{J} \left(\frac{1}{\sigma_j^2} \boldsymbol{A}_j^T \boldsymbol{P}_j \boldsymbol{l}_j \right) \right) \tag{8}$$

Moreover, we use the Monte-Carlo variance component estimation (MCVCE) to estimate the appropriate variance factors of different observation groups and the regularization parameter (Koch and Kusche, 2002; Kusche, 2003; Wu et al., 2017c).

3. Numerical results and discussion

3.1. Wavelet analysis of local gravity signals

In order to determine the depths of different layers, the residual gravity data are decomposed into the signals at different scales based on wavelet analysis. The spline interpolation is used to compute the gridded data, and Coif3 basis functions are chosen for wavelet decomposition (Xu et al., 2017). The preliminary maximum order for wavelet decomposition is arbitrarily chosen to some extent, however, since the low-order details are invariant with the increase of decomposition order, we can preliminarily choose a predefined order and implement the wavelet decomposition, and analyze the derived details. If there are still details that are useful for constructing the multilayer model haven't been separated, we need to increase the decomposition order until all the useful details have been extracted; otherwise, we truncate to a specific order, and compute the wavelet details and approximation to construct the multiply layer's parameterization. By trial and errors, the preliminary order for decomposition is chosen as nine, and Figure 1 shows the derived wavelet details (the corresponding statistics are provided in Table 1). With the increase of decomposition order, more long-wavelength features occur. More specifically, the low-order details demonstrate the high-frequency signals stemmed from the shallow and small-scale substances; while, the high-order ones with long-wavelength patterns reflect the anomalies caused by deep and large-scale geological bodies. It is noticeable that the 1st- and

2nd-order details (i.e., D_1 and D_2) are seems dominated by the high-frequency signals correlate strongly with the local topography (the local digital terrain model (DTM) can be seen in Figure 1 in Wu et al. (2017c)). We mainly attribute this to the uncorrected topographical signals in RTM corrections, which is mainly due to the inaccuracy of the density parameters in RTM and limitations of DTM both in terms of spatial resolution and precision. As a result, the high-frequency signals originated from local topography variation cannot thoroughly recovered from RTM reduction, and consequently, the uncorrected signals leak into the 1st- and 2nd-order details. To avoid these high-frequency errors propagating into the final solution, we neglect these two wavelet details in designing the multiply layers' networks. Moreover, with the order increasing to nine, we notice D_9 obviously reveal the large-scale signals with the wavelengths of hundreds of kilometers. Given that the mean distance between the data in this target area is approximately several kilometers and the spatial resolution of the applied GGM (i.e., GOCO05S) is roughly 72 km, the spectral contents of the residual signals need to be recovered is roughly between several kilometers and tens of kilometers within the RCR framework, i.e., approximately between degree 250 to 3000 in terms of spherical harmonics' representation. While, the spectral contents of the 9th-order details exceed the frequency bands of the signals need to be modeled, and the maximum order for wavelet decomposition is truncated to eight. In this manner, the third- to eighth-order (D_3 - D_8) wavelet details and the final approximation (A_8) (see the information in Figure 2 and Table 2) are applied for constructing the multilayer model, consists of seven layers at various depths.

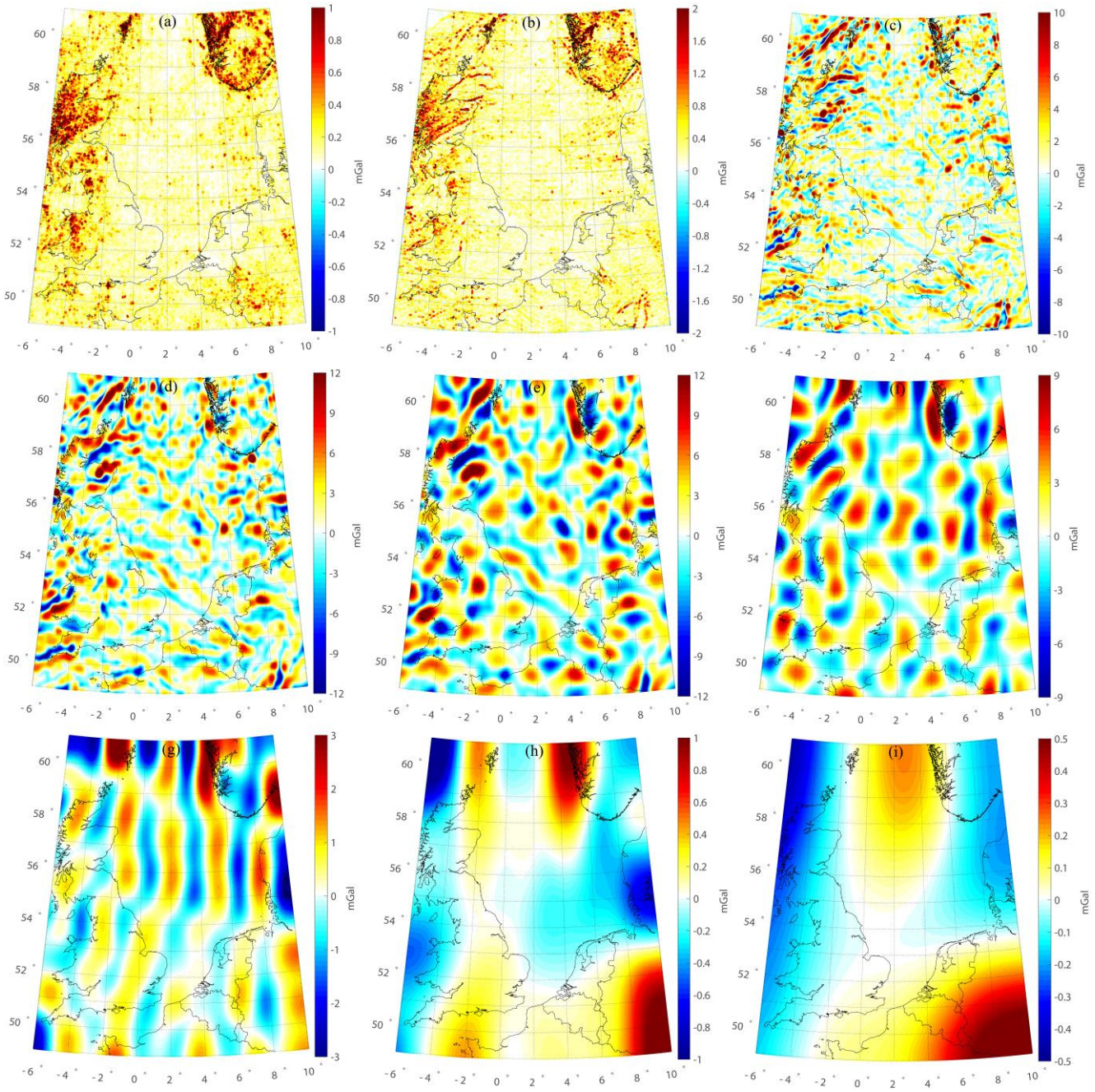

Figure 1. Wavelet details at various scales. (a) D_1, (b) D_2, (c) D_3, (d) D_4, (e) D_5, (f) D_6, (g) D_7, (h) D_8, and (i) D_9.

Table 1. Statistics of different wavelet details (units: mGal)

	max	min	mean	sd
D_1	2.23	-2.78	0.00	0.20
D_2	4.52	-5.57	0.00	0.32
D_3	19.27	-16.26	0.00	2.30
D_4	21.71	-17.46	0.00	3.18
D_5	15.38	-16.47	0.00	3.80
D_6	10.60	-9.72	0.00	2.75
D_7	4.43	-3.33	0.00	0.95
D_8	1.23	-1.52	0.00	0.34
D_9	0.66	-0.45	0.00	0.18

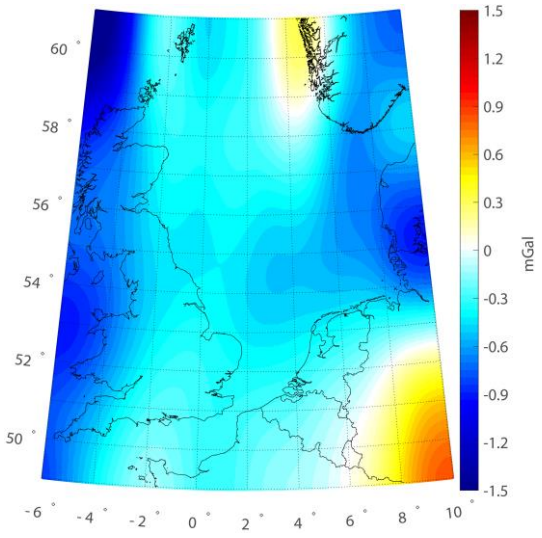

Figure 2. Wavelet approximation A_8 .

Table 2. Statistics of wavelet approximation (units: mGal).

max	min	mean	sd
0.83	-1.70	-0.41	0.32

3.2. Key parameters of Poisson wavelets

The order of Poisson wavelets is fixed at 3 to achieve a good compromise between the localization in space and frequency domain (Panet et al., 2011). In addition, the depth and number of Poisson wavelets are the crucial points affecting the solution quality (Klees et al., 2008). Poisson wavelets belong to different layers are placed on the Fibonacci grids at various depths beneath the topography, and the power spectrum analysis is applied to estimate the depths. As shown in Figure 3, the green curves show the radially averaged logarithm power spectrums of signals at different scales, and the red straight lines represent the slopes of the spectrums, indicate the depths of corresponding layers. The red lines represent rates of change for logarithmic power relative to wave number, estimated by a autoregressive method; and the starting point and terminal point of the red lines are the inflection points of the curves, recognized according to the trend of the curves (Xu et al., 2018). The layers go deeper as the scales increase, and the shallow layers reflect the small-scale signals, while the deep ones recover the long-wavelength information. Table 3 provides the estimated depths of different layers, limited between 4 and 60 km. The shallowest layer locates 4.5 km underneath the topography, while the depth of the deepest one is approximately estimated as 59.2 km. It is noticeable that the thickness of sediments in this area is approximately 2~4 km, and the thickness of the upper-middle crust is roughly 15~20 km (Artemieva and Thybo, 2013). Thus, the first four layers (layer1, layer2, layer3 and layer4) locate between the sediments and upper-middle crust, and the corresponding wavelet details (D_3 , D_4 , D_5 and D_6) display as the small-scale patterns due to the highly heterogeneous structure of the crust. The distributions of D_3 and D_4 (with the average depths of 4.5 km and 9.2 km, respectively) on land are more dispersed than that in the ocean, demonstrate that the tectonic structure underneath the land is more complex than that beneath the ocean in the upper crust. Moreover, the gravity anomalies in the northern of North Sea are more dispersed than those in the central and southern of North Sea, which is consistent with that the Viking Graben and basin are located in the northern and southern of North Sea, respectively, e.g., see Fichler and Hospers (1990), and Blundell et al. (1991). The mean source depths of D_5 and D_6 are 13.7 km and 19.6 km, respectively, correspond to the depths of the middle crust. The gravity

anomalies during these two layers present apparent positive-negative alternating patterns, which may be interpreted as the crustal shearing and extrusion (Blundell et al., 1991; Ziegler and Dèzes, 2006). While, the last three layers (layer5, layer6, and layer7) are supposed to be located between the Moho surface and upper mantle considering the Moho depth in this region is approximately 25~30 km (Grad and Tiira, 2009), and the corresponding details (D_7 , D_8 and A_8) become smoother and more long-wavelength signals occur. D_7 with the mean source depth of 27.0 km primarily reflects the Moho undulation. The distribution of positive-negative alternating gravity anomalies in D_7 is nearly south-north oriented, which is in agreement with the features of the Moho relief in this area (Fichler and Hospers, 1990; Ziegler and Dèzes, 2006). The average source depths of D_8 and A_8 are 32.3 km and 59.0 km, respectively, correspond with the depth of the upper mantle, indicate that the density distribution of the upper mantle is relatively smooth. Overall, these decomposed gravity anomalies can reveal the tectonic structure of study area at different depths.

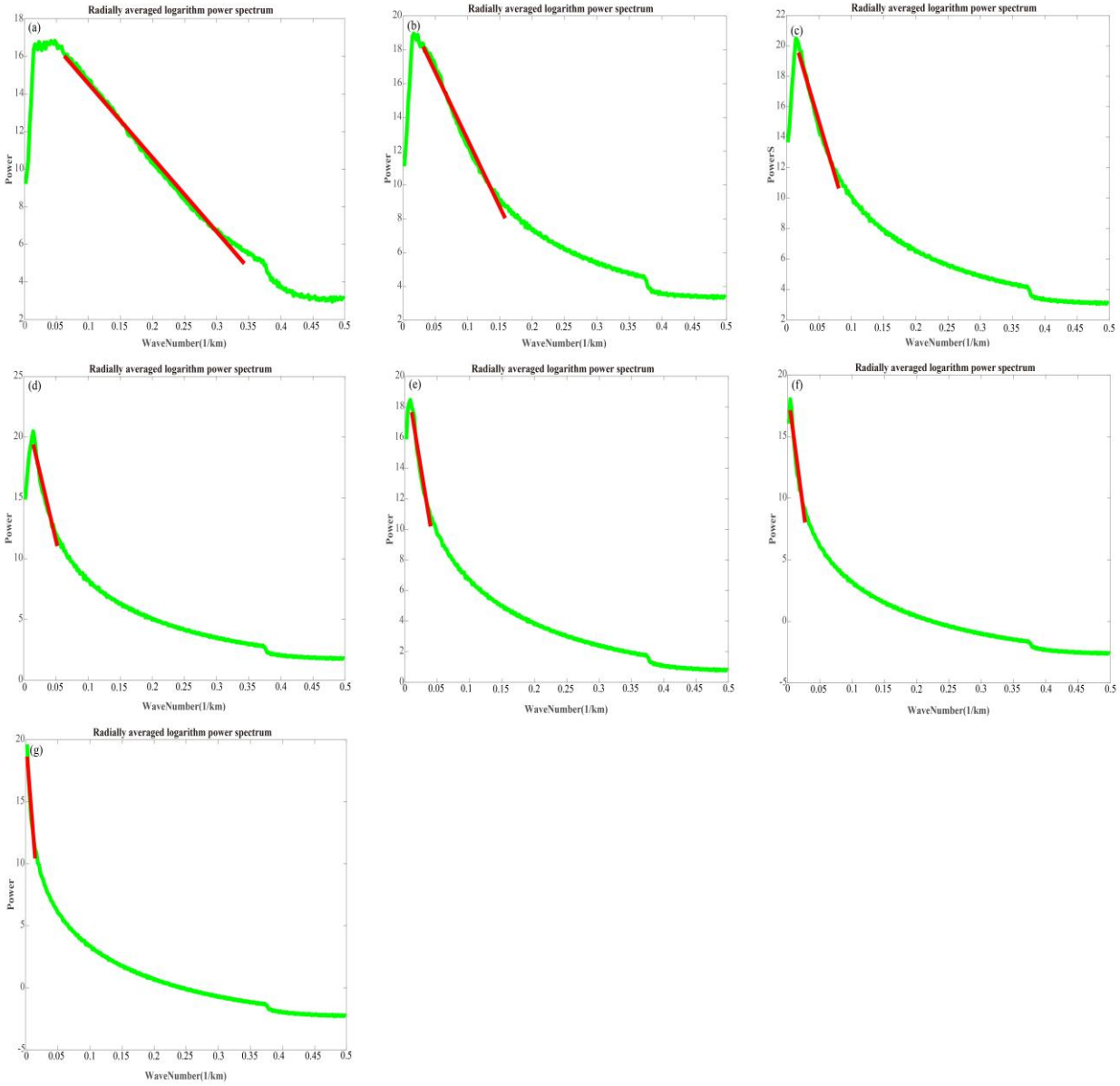

Figure 3. Power spectrum analysis of various wavelet signals. (a) D_3, (b) D_4, (c) D_5, (d) D_6, (e) D_7, (f) D_8, and (g) A_8.

The green curves are the radially averaged logarithm power spectrums, and the red straight lines represent rates of change for logarithmic power relative to wave number..

5

Table 3 Depths of multiply layers beneath the topography (Units: km).

layer1	4.5
layer2	9.2
layer3	13.7
layer4	19.6
layer5	27.0
layer6	32.3
layer7	59.2

As mentioned above, different layers are designed to recover the wavelet details and approximation at different scales, and a trial-and-error approach is used to estimate the number of Poisson wavelets of each layer (Wittwer, 2009). For a specific layer with the fixed depth, we predefine different number of Poisson wavelets to form a certain number of Fibonacci grids. Then, the signals reconstructed from these grids are compared with the true values, i.e., ones derived from wavelet decomposition, and the parameter that derives the smallest differences between the modeled and true signals is consider as the optimal one. By trail and errors, the spatial resolutions of Fibonacci grids (mean distance between Poisson wavelets) are changed from 20 to 14 km with a step of 1 km. Table 4 shows the accuracies of the solutions derived from different Fibonacci grids of multiply layers, and we take the situation of the first layer for instance. With the increase of Poisson wavelets, the SD value of the differences between the reconstructed and true signals decreases gradually to 0.12 mGal when the spatial resolution of the grid increase to 16 km. Since then, no significant improvements occur with incorporating more Poisson wavelets. Moreover, introducing more Poisson wavelets increases the overlapping between them, which may lead to the highly-conditioned normal matrices, and the associated heavy regularization may decrease the solution quality (Wu et al., 2017b). The optimal mean distance between Poisson wavelets of the first layer is estimated as 16 km. Similarly, the spatial resolutions for the rest layers can be determined in this way, see Table 4.

Table 4 Accuracies of solutions derived from various Fibonacci grids of different layers (Units: mGal).

	20 km	19 km	18 km	17 km	16 km	15 km	14 km

layer1	0.43	0.34	0.21	0.16	0.12	0.12	0.12
layer2	0.52	0.43	0.33	0.25	0.19	0.16	0.16
layer3	0.58	0.40	0.28	0.19	0.16	0.14	0.14
layer4	0.55	0.39	0.29	0.26	0.15	0.13	0.13
layer5	0.38	0.26	0.17	0.14	0.10	0.10	0.10
layer6	0.22	0.16	0.12	0.10	0.08	0.08	0.08
layer7	0.11	0.09	0.08	0.06	0.06	0.06	0.06

3.3. Regional solution and its validation

For regional gravity field recovery, point-wise terrestrial and shipboard gravity anomalies are combined. Since there are no accurate information for terrestrial and shipboard data, we assume the accuracies of 2 mGal for both of these two types of data, and the posterior variance factors of different observation groups are estimated from MCVCE method. The weights of different observation groups, indicate their relative contributions, and play a key role in data combination. The estimated variance factors for terrestrial and shipboard gravity data are approximately 1.45 mGal and 1.30 mGal through the MCVCE method, respectively, when we model the local gravity field based on the multilayer approach. For terrestrial data, the estimated accuracy is in good agreement with that derived by Klees et al. (2008), i.e., 1.48 mGal for parts of the Netherlands. However, it is difficult to judge whether this estimate is realistic in other regions because of a lack of accuracy information. While, for shipboard data, the computed value of 1.30 mGal is smaller than the results of crossover adjustments, where the standard deviation for the residuals at the crossovers was approximately estimated as 2.0 mGal (Slobbe, 2013). However, this value may be too optimistic considering much of the shipborne data were collected decades ago without GPS navigation. The first-order Tikhonov regularization is used to tackle the ill-conditioned problem (Kusche and Klees, 2002; Wu et al., 2017b), and the convergent regularization parameter is approximately 0.5×10^{-5} estimated from the MCVCE method; the details for regularization parameter estimation and comparisons with different methods can be referred to Wu et al. (2017b).

The performance of the traditionally-used single-layer is also investigated for comparison, and the parameterization of local gravity field based on the single-layer approach can be seen in, e.g., Klees et al. (2008) and Slobbe (2013). By trial and errors, the single layer of Poisson wavelets' grid is located 40 km beneath the topography, and the mean

distance between Poisson wavelets is defined as 8.7 km (Wu et al., 2016). Figure 4 shows the normalized spectrums for different approaches. Considering the frequency range of the signals to be recovered in the target area is approximately between degree 250 to 3000 in spherical harmonics' representation, we note the single-layer approach is only sensitive to parts of the signals' spectrum, i.e., approximately between degree 300 to 1200 if we suppose half of the maximum value of the normalized spectrum is the criterion for determining whether it is sensitive or not within a specific frequency band. However, for the high-frequency band between degree 1200 to 3000, this approach is less sensitive. On the contrary, the multilayer approach effectively covers the spectrum of the local gravity signals, which is both sensitive to the low- and high-frequency bands. Figure 5 provides the residuals of data after least squares adjustment using different methods, shows the residuals derived from the multilayer approach reduce significantly in the whole region compared with ones obtained from the single-layer approach, especially in western parts of UK, south of Norway, and southwest of Germany, where the high-frequency signals correlated with local topography dominate the features of regional gravity field. We also find the improvements occurring in the ocean parts, especially in waters around the English Channel, Irish Sea, northwest of North Sea, and Atlantic Ocean close to northwest UK. The statistics in Table 5 displays the standard deviation (SD) value for the residuals of terrestrial (shipborne) gravity anomalies decreases by 0.39 mGal (0.36 mGal) when the multilayer approach is used. These results are reasonable since the multilayer approach contains several layers shallower than 40 km, and the spectrums of these layers shift to the high-frequency bands. As a result, the spectrum of the multilayer approach is more sensitive to signals with high-frequency properties, and consequently, the local high-frequency signals can be better fitted by the multilayer approach. It is also worth to mention that the analysis of data residuals can't be treated as the only criteria for justifying the performances of different approaches, since these gravity data have been used for modeling purpose, and the SD values of data residuals should be regarded as the internal agreement. Besides, due to the limitation of the accuracies of gravity data, we can't make conclusions too firmly only depends on the analysis of data residuals. One may also argue that it may be possible to derive lower data residuals if we put the Poisson wavelets' grid shallower when the single-layer approach is used. However, we believe a shallower single grid may reduce the data residuals, but may not derive a better solution when validated against the independent control data, see the detailed discussions in Wu et al. (2016). In the following part, we introduce another high-quality independent data set, i.e., GPS/leveling data, for external validation, which give us more confidences with respect to the performances of different methods.

It is also of interest to implement a Akaike information criterion (AIC) test for different models. Although, the

multilayer model fits the gravity observations better, but it also increases the level of estimated parameters. AIC rewards the goodness of fit of data, but also includes a penalty with the increasing of the number of estimated parameters. In other words, it deals with the trade-off between the goodness of fit of the model and the simplicity of the model. AIC value is an estimator of the relative quality of statistical models for a given set of data, providing a means for model selection, and the model that gives the minimum AIC value may be more preferable (Akaike, 1974; Burnham and Anderson, 2002). The definition for the AIC value can be seen in Eq.(A1) in the Appendix. Since we model the gravity field in the framework of least squares system, we can simply take $AIC = 2k + n\ln(RSS/n)$ for model comparision, where k is the number of estimated parameters in the model, n is the number of observations, and RSS is the residual sum of squares (RSS), see the details in the Appendix. In this study, the number of point-wise gravity observations used for modeling is 894649, and the numbers of estimated parameters in the multilayer and single-layer model are 47504 and 19477, respectively. The RSS values for the multilayer and single-layer model are computed as $8.8527\times10^{5}\ mGal^{2}$ and $1.3296\times10^{6}\ mGal^{2}$, respectively, based on the data residuals after the least squares adjustment. Then, the AIC values for the multilayer and single-layer model are estimated as 85581 and 393400, respectively. Based on these statistics, we notice that the multilayer model gives a smaller AIC value, which may be more preferable since it reaches a better balance between the goodness of fit of data and the simplicity of the model.

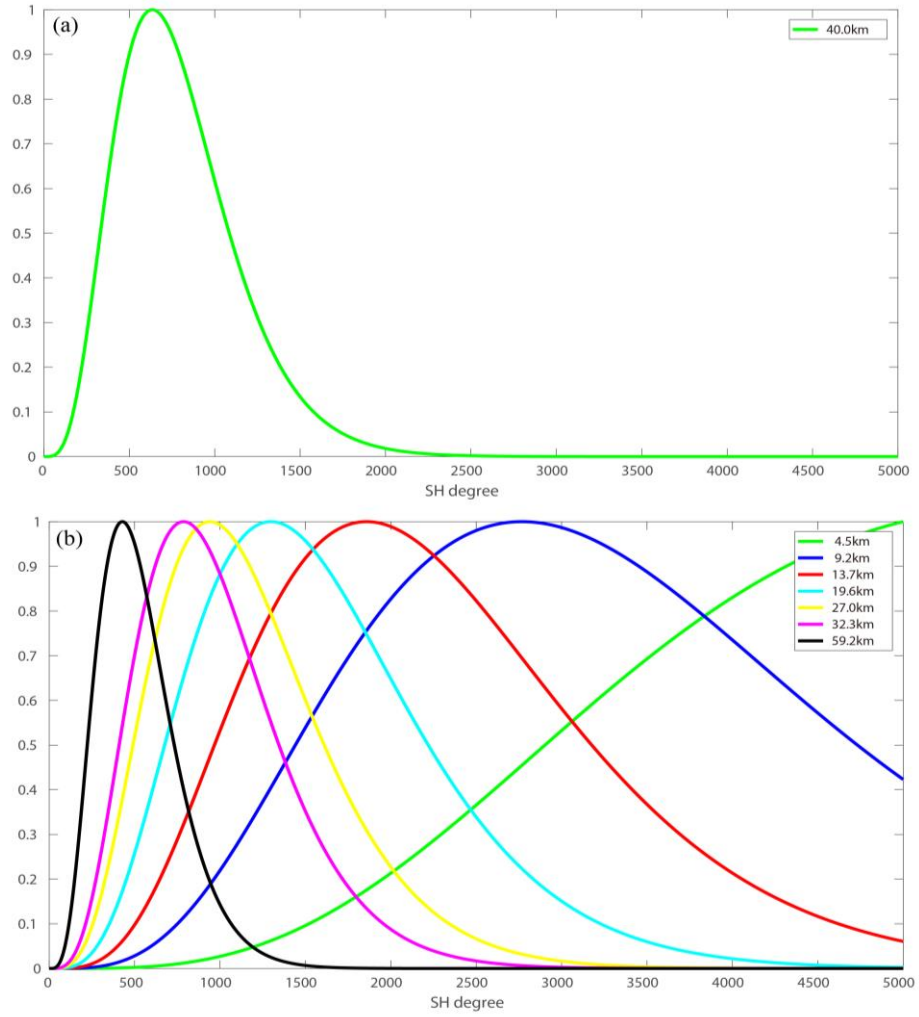

Figure 4. Normalized spectrums for (a) single-layer and (b) multilayer approach.

To test the ability of realistic extrapolation of different regional models recovered from various methods, which is actually comparing the predicted values derived from the regional model (e.g., model computed from the multilayer or single-layer approach) and ones derived from independent survey/measurements, we introduce GPS/leveling data in the Netherlands (534 points), Belgium (2707 points), and parts of Germany (213 points) as the independent validation data. These data are provided in terms of geometric quasi-geoid heights derived from the high-quality GPS measurements and leveling survey, and the overall estimated accuracy of these observed quasi-geoid heights is approximately at 1 cm level. It is worth to mention that these GPS/leveling data are not combined for modeling, and

their three dimensional coordinates don't coincide with the positions of gravity data. For validating different models with GPS/leveling data, we need to reconstruct the regional model based on the computed Poisson wavelets' coefficients and coordinates of GPS/leveling points (see Eq.(6)), and compute the gravimetric quasi-geoid heights at these points, which are ones predicted from the regional model. Then, we compute the standard deviation (SD) of the point-wise difference between GPS/leveling data and the gravimetric quasi-geoid height derived from the regional approach, which is actually external validation. The validation results demonstrate the discrepencies between the GPS/leveling points and quasi-geoid heights derived from the multilayer approach decrease substantially compared with ones computed from the single-layer approach, see Figure 6. The most prominent improvements occur in the northwest of Belgium, west of Germany, and eastern parts of Netherlands, which are in good agreement with the results for data residuals analysis demonstrated in Figure 5. As shown in Table 6, the accuracies of gravimetric quasi-geoid derived from the multilayer approach are improved by 0.4 cm, 0.9 cm and 1.1 cm in the Netherlands, Belgium and parts of Germany, respectively. Moreover, the mean values indicate that the solution computed from the multilayer approach further reduces the biases between gravimetric solution and local GPS/leveling data, with the magnitude of 0.8 cm, 0.7 cm, and 1.1 cm in these three regions, respectively, compared to the one modeled from the single-layer approach. From these results, we can see that the multilayer approach not only leads to a reduction for the data residuals, but also derives a better solution assessed by the independent control data, compared to the single-layer approach. For constructing the multilayer model, we consider that the gravity signals are the sum of the contributions generated from the anomaly sources, and different layers are designed for recovering these contributions with heterogeneous spectral contents. As a result, the spectrum of multilayer approach is sensitive to the frequency bands of local gravity signals, both in low- and high-frequency bands, and the local signals may be better recovered. We also notice that there are still biases between the regional gravimetric solutions and local GPS/leveling data, see the mean values in Table 6, which are mainly due to the commission errors in the GGM and uncorrected systematic errors in the local gravity data and leveling systems (Fotopoulos, 2005). Generally, corrector-surface (Fotopoulos, 2005; Nahavandchi and Soltanpour, 2006) or more complicated algorithms, like least squares collocation (Tscherning, 1978), boundary-value methodology (Klees and Prutkin, 2008; Prutkin and Klees, 2008), and a direct approach (Wu et al., 2017a), can be applied to reduce the systematic errors and properly combine GPS/leveling data and gravimetric solution. However, since the target for this study is to develop a multilayer approach for gravimetric quasi-geoid modeling, which is served as a basic surface for further geophysical applications, e.g., study the ocean circulation and structure of lithosphere; while, after implementing these methods for combining local GPS/leveling and gravimetric

model, the derived quasi-geoid is not purely gravimetric. Besides, we only have the well distributed GPS/leveling data in the limited region, i.e., in Netherlands, Belgium, and parts of Germany, while in other regions, no high-quality control data are available. If we use the locally distributed GPS/leveling data for removing these systematic errors and computing the combined quasi-geoid, the final solution may be distorted in other regions, especially in the ocean parts, since no control data in these regions have been combined. Thus, we don't implement these methods mentioned above for computing the combined quasi-geoid. In following study, we use the gravimetric model derived from the multilayer approach, which is hereafter denoted as QGNSea V1.0 (quasi-geoid over the North Sea version 1.0).

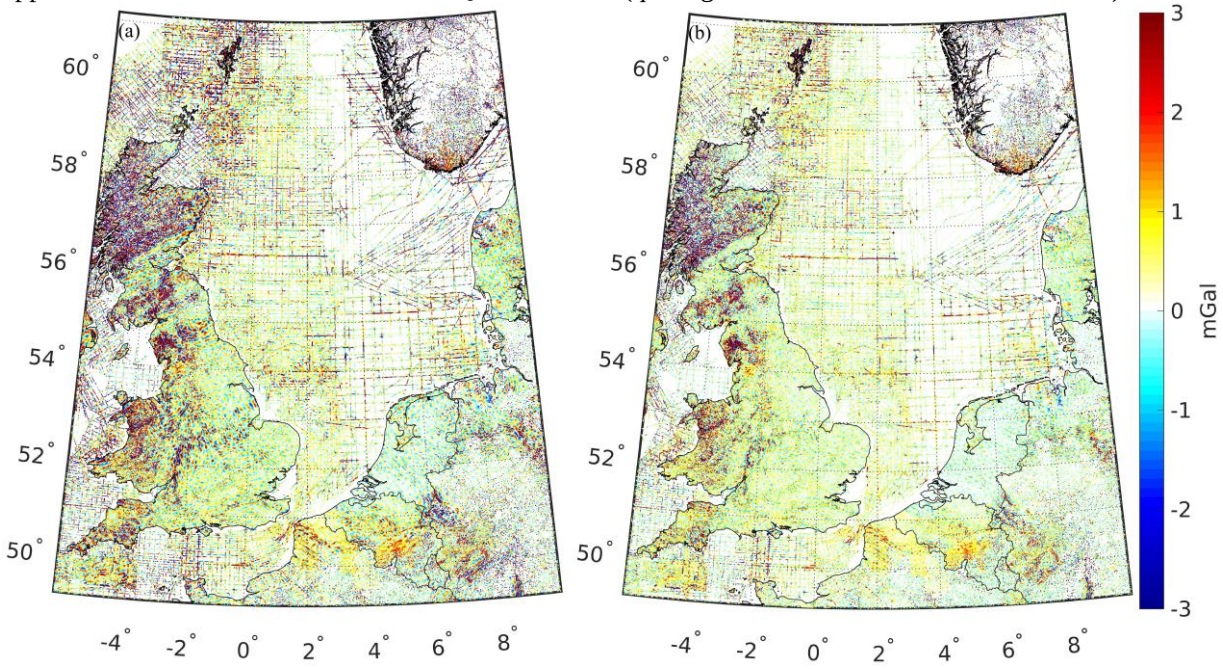

Figure 5. Residuals of gravity data derived from (a) single-layer and (b) multilayer approach.

Table 5 Statistics of residuals of gravity data computed from different approaches (units: mGal).

		max	min	mean	sd
Single-layer approach	Terrestrial	19.58	-16.91	0.00	1.45
	Shipborne	11.91	-17.38	0.00	1.07
Multilayer approach	Terrestrial	16.96	-14.90	0.00	1.06
	Shipborne	9.25	-15.96	0.00	0.71

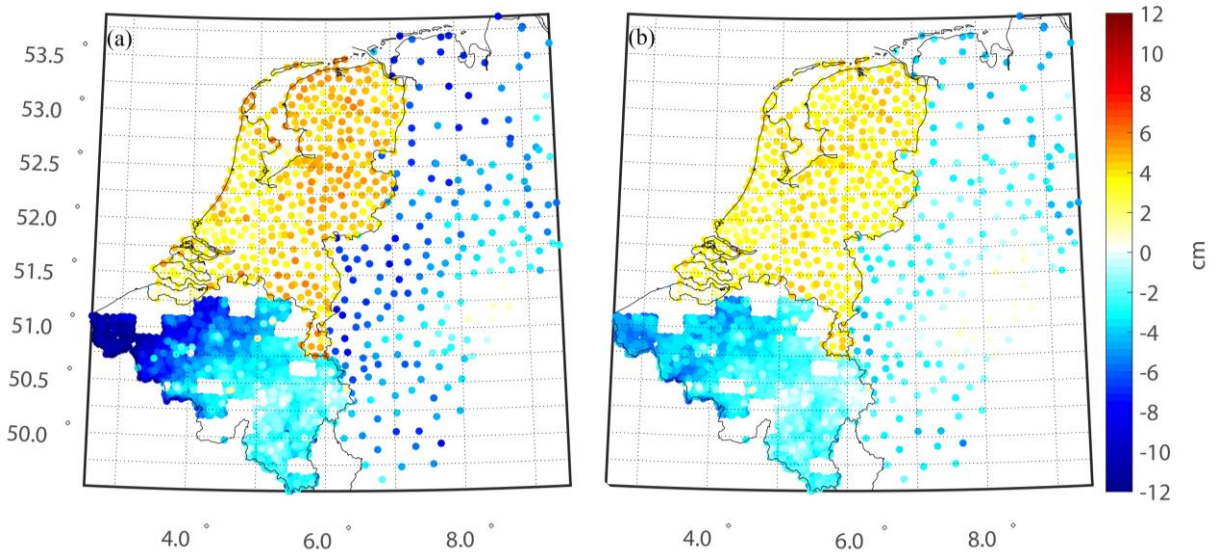

Figure 6. Differences between GPS/leveling data and gravimetric quasi-geoids computed from (a) single-layer and (b) multilayer approach.

Table 6 Evaluation of quasi-geoids modeled from different approaches (Units: cm).

		max	min	mean	sd
Single-layer approach	Netherlands	5.9	0.1	3.8	1.2
	Belgium	1.2	-13.1	-3.5	2.8
	Germany	1.2	-11.2	-3.6	2.9
Multilayer approach	Netherlands	4.8	0.0	3.0	0.8
	Belgium	1.2	-6.8	-2.8	1.9
	Germany	1.0	-6.7	-2.5	1.8

QGNSea V1.0 is compared with a regional model called EGG08 (Denker, 2013) and other four recently published high-order GGMs, i.e., EGM2008 (d/o 2190) (Pavlis et al., 2012), EIGEN-6C4 (d/o 2190) (Förste et al., 2014), GECO (d/o 2190) (Gilardoni et al., 2015), and SGG-UGM-1 (d/o 2159) (Liang et al., 2018), for further comparisons. The reason for choosing these four GGMs for comparisons is that these models have relatively higher spatial resolutions and better accuracies compared to most of other available GGMs, see the information in http://icgem.gfz-potsdam.de/home. EGG08 is a regional gravimetric quasi-geoid model in Europe, which was

recovered by stokes integral based on locally distributed gravity data. This model is provided in terms of gridded data instead of spherical harmonics, the space resolution of which is 1′ in latitude and 1.5′ in longitude, respectively (Denker, 2013). While, the rest four models are global geopotential models provided in terms of spherical harmonics, and EGM2008 was computed by merging GRACE measurements, terrestrial, altimetry-derived, and airborne gravity data. Since no GOCE data have been incorporated for developing EGM2008, and the recently published GGMs have been developed by combining GOCE data, which is supposed to improve the gravity field in the frequency bands approximately from degree 30 to 220 in spherical harmonics representation (Gruber et al., 2010). EIGEN-6C4 was computed by combining GRACE, GOCE, and terrestrial gravity data and other data sets; GECO was computed by incorporating the GOCE-only TIM R5 (d/o 250) solution into EGM2008, and SGG-UGM-1 was computed by the combination of EGM2008 gravity anomalies and GOCE gravity gradients and satellite-to-satellite tracking data. Differences between QGNSea V1.0 and other models are shown in Figure 7 (the boundary limits for the area are contracted by 0.5 ° in all the directions to reduce edge effects), the magnitude of which reaches decimeter level. For EGG08, we note the most prominent differences appear in eastern parts of the Irish Sea and center of Germany. Different data pre-processing procedures and methods for parameterization partly account for these differences, e.g., QGNSea V1.0 is recovered from the multilayer approach using Poisson wavelets and proper weights for different observation groups are estimated through MCVCE; while the spectral combination technique and spectral weights were implemented in EGG08 for merging heterogeneous data (Denker, 2013). Larger differences are observed between QGNSea V1.0 and these four GGMs, and remarkable differences show in southern of Norway, northern of the North Sea, eastern of the Irish Sea, and northwest of Germany; besides from the applications of different techniques for modeling, these differences are partly interpreted as the additional signals introduced by QGNSea V1.0, stemming from the incorporation of more high-quality gravity data. The evaluation results with GPS/leveling data displayed in Figure 8 and Table 7 show the gravimetric quasi-geoid inversed from the multilayer approach has the best quality, especially in the north of the Netherlands and western and eastern parts of Belgium. The SD value of the misfit between the GPS/leveling data and QGNSea V1.0 is 1.5 cm, while this value increases to 2.2 cm when EGG08 is validated. In contrast, the accuracies of these four GGMs are slightly worse than EGG08, which are approximately at 2.6 cm levels. Compared to these GGMs, the added values introduced by the local high-quality data lead to the primary improvements of QGNSea V1.0. We find that these four GGMs have the comparable accuracies, where the ones developed by combining GOCE data and EGM2008 (i.e., GECO and SGG-UGM-1) don’t have better performances than EGM2008, and SGG-UGM-1 even has the slightly worse performance than EGM2008, which is especially

prominent in the eastern parts of Belgium, however, the possible reasons need further investigation. We also notice that a new Europe gravimetric quasi-geoid called EGG2015 has been computed, where the GOCE-derived GGMs were used as the reference models (Denker, 2015). However, this model is not publicly available, and its performance can't be assessed in this local region.

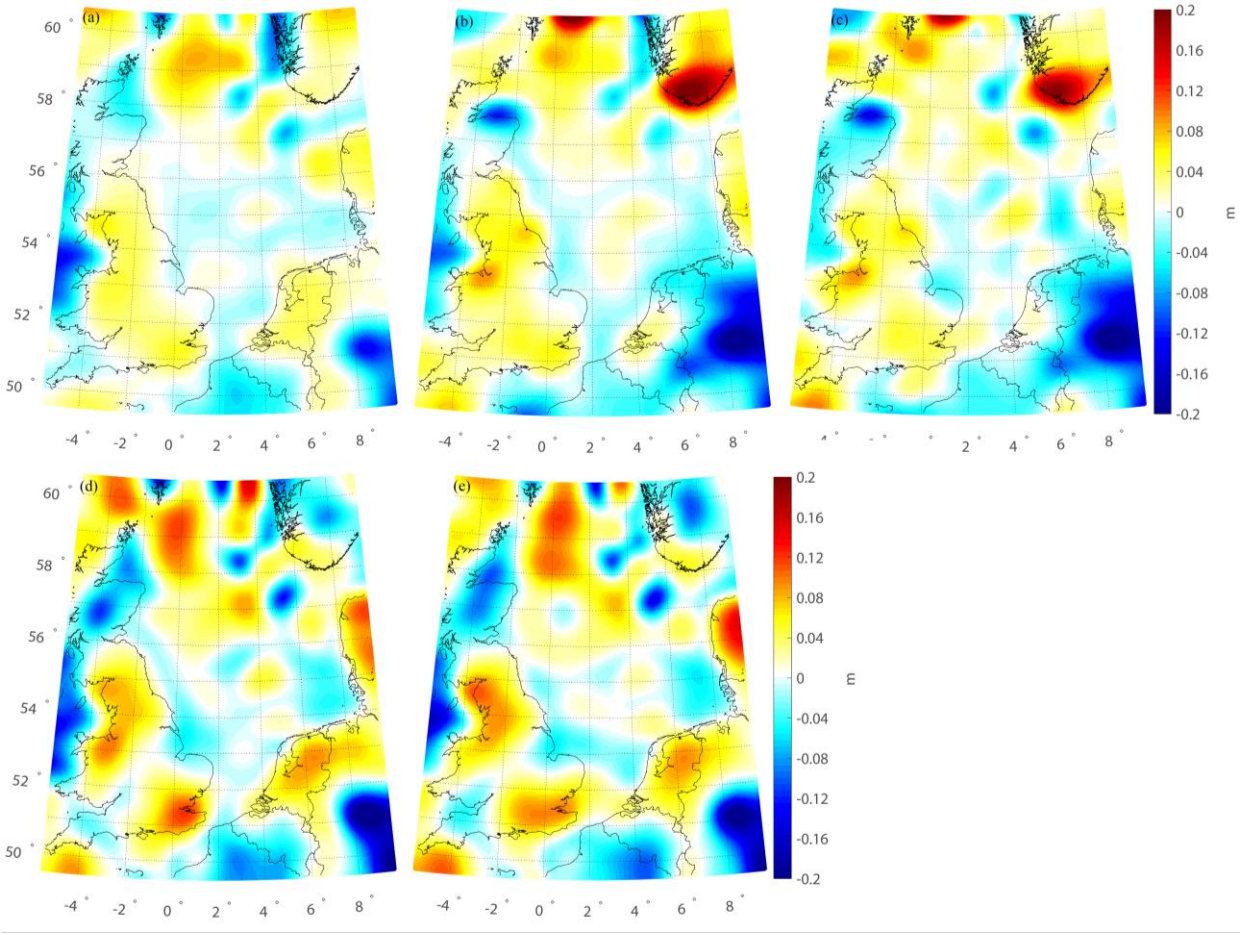

Figure 7. Difference between QGNSea V1.0 and (a) EGG08, (b) EGM2008, (c) EIGEN-6C4, (d) GECO, (e) SGG-UGM-1. Note that the mean differences are removed.

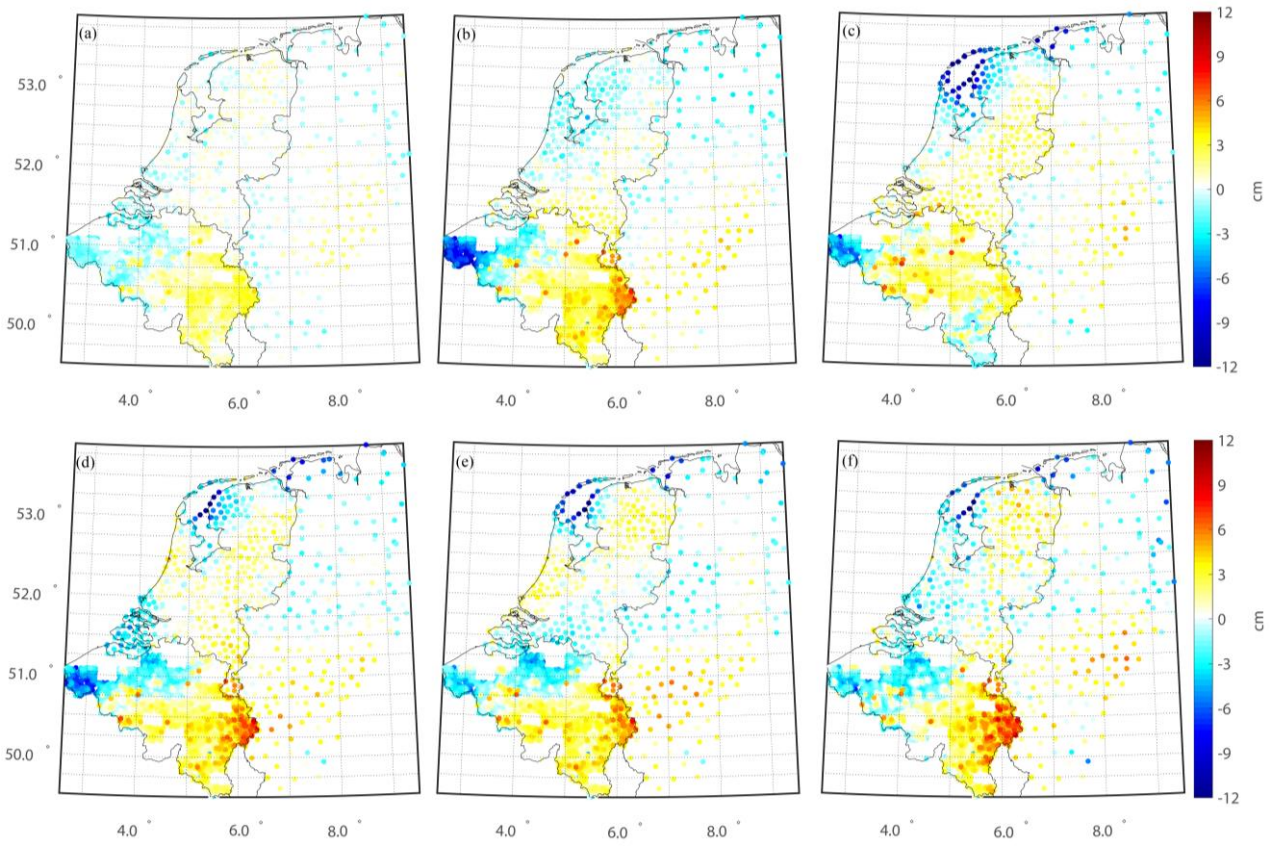

Figure 8. Evaluation of the various quasi-geoids. (a) QGNSea V1.0, (b) EGG08, (c) EGM2008, (d) EIGEN-6C4, (e) GECO, and (f) SGG-UGM-1. Note that the mean differences are removed.

Table 7. Statistics of accuracy of various quasi-geoids. (units: cm). Note that the mean differences are removed.

	max	min	sd
QGNSea V1.0	5.2	-3.9	1.5
EGG08	7.8	-9.4	2.2
EGM2008	8.4	-10.0	2.6
EIGEN-6C4	9.0	-11.9	2.7
GECO	8.3	-12.8	2.6
SGG-UGM-1	8.8	-12.7	2.7

For further comparisons, we compute the local mean dynamic topography (MDT), which illustrates the departure of

the mean sea surface (MSS) from the quasi-geoid/geoid (Becker et al., 2014; Bingham et al., 2014). We compute the MDTs in a geodetic way, and the raw MDTs are computed as the differences between MSS and local geoid/quasi-geoid models, and the derived MDTs are further smoothed with a Guassian filter to suppress the small-scale signals that can't be resolved from the MSS or local geoid/quasi-geoid (Andersen et al., 2013). DTU13MSS from 1993-2012 is chosen as the MSS, and this model is provided as the gridded data, with the spatial resolution of 1′×1′ (Andersen et al., 2013). Considering QGNSea V1.0 and EGG08 have better performances than other models compared with local GPS/leveling data, we only compute the local MDTs based on these two gravimetric quasi-geoids. DTU13MSS and QGNSea V1.0/EGG08 are directly combined to obtain the raw MDT. Then, a Gaussian filter with a correlation length of 6 km is further applied to smooth the derived MDT, considering the small-scale signals that have the wavelengths shorter than several kilometers can't be recovered from the local gravity data, since the mean distance between gravity data is approximately at 6~7 km level. The modeled MDTs based on QGNSea V1.0 and EGG08 are denoted as MDTNS_QGNSea and MDTNS_EGG08, respectively, see Figure 9, showing in good agreement with each other in most areas over the North Sea. Prominent signals like the Norwegian coastal currents can be seen in these two MDTs, also see e.g., Idžanović et al. (2017), although the signals observed in MDTNS_QGNSea don't provide a full picture of Norwegian coastal currents due to the limited data coverage in Norway and its neighbouring ocean areas. While, in other areas of the North Sea, the MDTs show quite smooth patterns, indicate the small change in sea surface topography, which is consistent with Hipkin et al. (2004). However, extreme values are observed surrounding most offshore areas, e.g., see the features over the offshore regions closed to The Wash (around 0.5 °W and 53 °N) and Thames estuary (around 1 °W and 51.5 °N) in England, and along the coastal areas of France, Netherlands, and Germany, which are typically identified as errors (Hipkin et al., 2004). The problems for computing geodetic MDTs in offshore regions are twofold. First, the quasi-geoid/geoid is poorly modeled in coastal areas due to the unfavorable data coverage, and data inconsistencies are usually observed when combining land and marine gravity surveys. Moreover, the quality of altimetry data is dramatically reduced near the offshore areas, and associated errors in the derived MSS propagate into the final MDT (Andersen et al., 2013). However, airborne gravity measurements provide a seamless way for gravity measurements over land and seas, which may allay this situation (Andersen and Knudsen, 2000).

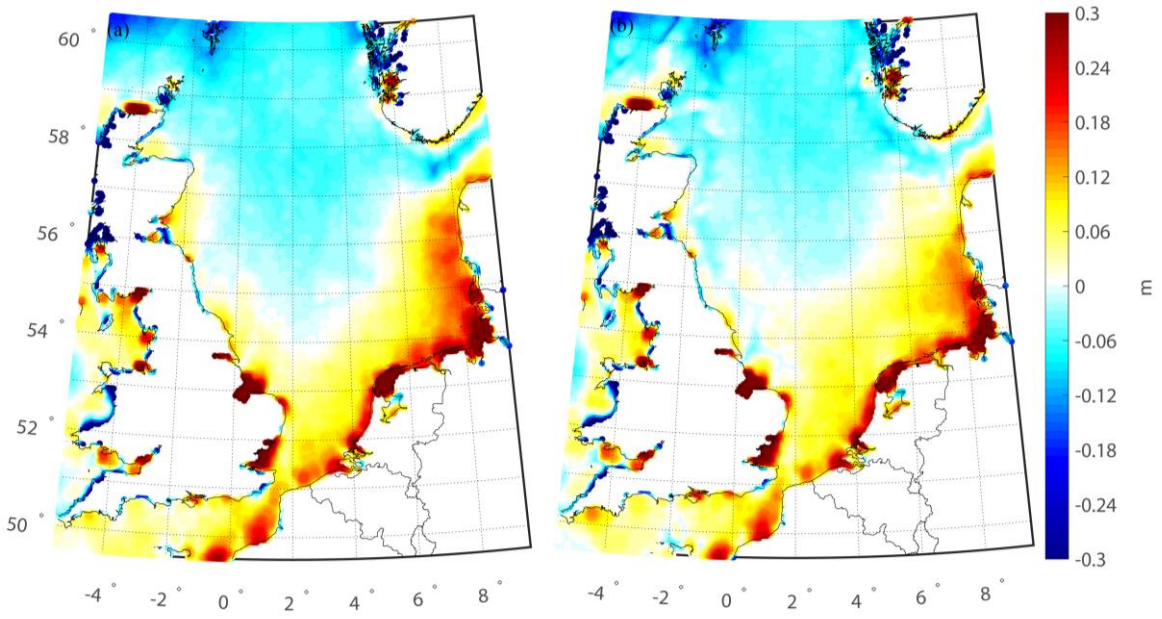

Figure 9. Different geodetic MDTs in North Sea. (a) MDTNS_QGNSea; (b) MDTNS_EGG08. For all profiles the mean value has been removed.

4. Conclusions

A multilayer approach is developed for gravity field recovery at regional scales in the framework of multi-resolution representation, where the residual gravity field is parameterized as the superposition of the multiply layers of Poisson wavelets located at the different depths beneath the topography. Since the gravity signals is the sum of the contributions generated from the anomaly sources at different depths, we put the multiply layers at the locations where different anomaly sources situate. Further, wavelet decomposition and power spectrum analysis are applied for estimating the depths of different layers.

For testing the performance of this multilayer approach, a local gravimetric quasi-geoid called QGNSea V1.0 over the North Sea in Europe is modeled and compared with other models. Based on wavelet decomposition and power spectrum analysis, multiply layers that situate between 4.5 km and 59.2 km underneath the topography are built to capture the signals at different scales. The numerical results show that the multilayer approach is sensitive to the spectrum of signals, both in the low- and high-frequency bands; while, the traditionally-used single-layer approach is only sensitive for parts of signals' spectrum. The comparisons with the single-layer approach show that the multilayer

approach fits the gravity observations better, especially in the regions where the gravity signals show strong correlations with the variation of local topography. Moreover, we introduce a Akaike information criterion (AIC) test for different models, which is an estimator of the relative quality of statistical models for a given set of data, providing a means for model selection in the view of statistical test. The associated results demonstrate that the multilayer model gives a smaller AIC value, which reaches a better balance between the goodness of fit of data and the simplicity of the model. The evaluation with independent GPS/leveling data tests the ability of realistic extrapolation of regional models recovered from different methods, reveals the model called QGNSea V1.0 computed by multilayer approach fits the local GPS/leveling data better, by the magnitudes of 0.4 cm, 0.9 cm and 1.1 cm in the Netherlands, Belgium and parts of Germany, respectively, compared to the one recovered from the single-layer approach. Further comparisons with the existing models show that QGNSea V1.0 has the best performance, which may be beneficial for investigating the ocean circulation in the North Sea and surrounding oceanic areas.

Future work is needed for further improving the QGNSea V1.0. First, the satellite data (e.g., K-band Range Rate data and gravity gradients) from GRACE and GOCE missions can be combined with the ground-based gravity data. However, deeper layers than ones we use to combine surface data may be implemented to incorporate satellite observations, since these data mainly contribute to low-frequency bands of gravity field. In addition, the stochastic model may need to be refined. For instance, the effects on the solutions caused by the GGM's errors may be quantified if the full error variance-covariance matrix of the spherical coefficients is incorporated into the stochastic model. In this way, the different data may be more properly weighted, and the solution may be further improved.

Author contributions. All authors have contributed to designing the approach and writing the manuscript.

Code and data availability. The source code is included as the Supplement. Gravity data were provided by the British Geological Service; the Geological Survey of Northern Ireland; the Nordic Geodetic Commission; Bundesamt für Kartographie und Geodäsie (Germany); Institut für Erdmessung (Germany); the Bureau Gravimétrique International IAG service (France); the Banque de données Gravimétriques de la France; and the Bureau de Recherches Géologiques et Minières (France). GPS/leveling data were provided by the Geo-information and ICT of Rijkswaterstaat (RWS-AGI) and the GPS Kernnet of the Kadaster, National Geographic Institute (NGI) and the Royal Observatory (ROB), and Bundesamt für Kartographie und Geodäsie.

Competing interests. The authors declare that they have no conflict of interest.

Acknowledgments. The authors would like to give our sincerest thanks to two anonymous reviewers and Dr. Cornelis Slobbe for their beneficial suggestions and comments, which are of great value for improving and correcting the manuscript. We also thank the Executive Editor Lutz Gross for the kind assistances and constructive comments. We thank the kind supports from the editorial office. We acknowledge funding from the Netherlands Vertical Reference Frame project. Thanks Prof. Roland Klees and Dr. Cornelis Slobbe from Delft University of Technology for kindly providing the original software, and part of the work was done in Delft University of Technology under the support with the State Scholarship Fund from Chinese Scholarship Council (201306270014). This study was also supported by China Postdoctoral Science Foundation (No.2016M602301), the Open Research Fund Program of the State Key Laboratory of Geodesy and Earth's Dynamics (No.SKLGED2018-1-2-E and SKLGED2018-1-3-E), Key Laboratory of Geospace Environment and Geodesy, Ministry of Education, Wuhan University (No.17-01-09), and National Natural Science Foundation of China (No.41504015).

Appendix A: Akaike information criterion

Suppose that we have a statistical model of some data, and the Akaike information criterion (AIC) value of the model is (Burnham and Anderson, 2002)

$$AIC = 2k\text{-}2\ln(\hat{L}) \tag{A1}$$

where k is the number of estimated parameters in the model, and $\hat{L}$ is the maximum value of the likelihood function for the model (Akaike, 1974; Burnham and Anderson, 2002).

For least squares fitting, the maximum likelihood estimate for the variance of a model's residuals distributions is

$$\hat{\theta}^2 = RSS / n \tag{A2}$$

where RSS is the residual sum of squares (RSS), and n is the number of observations.

Then, the maximum value of a log-likelihood function of least square model is (Burnham and Anderson, 2002)

$$-\frac{n}{2}\ln(2\pi) - \frac{n}{2}\ln(\hat{\theta}^2) - \frac{1}{2\hat{\theta}^2}RSS = -\frac{n}{2}\ln(RSS / n) + C \tag{A3}$$

where C is a constant independent of the model.

Combining Eq.(A1) and Eq.(A3), for least square model, the AIC value is expressed as

$$AIC = 2k + n\ln(RSS / n) + C \tag{A4}$$

Since only differences in AIC are meaningful, the constant C can be ignored, and we can conveniently take

$AIC = 2k + n\ln(RSS / n)$ for model comparisons.

References

Akaike, H.: A new look at the statistical model identification, IEEE Transactions on Automatic Control, 19(6), 716-723, doi:10.1109/TAC.1974.1100705, MR 0423716, 1974.

Andersen, O. B., and Knudsen, P.: The role of satellite altimetry in gravity field modeling in coastal areas, Phys. Chem. Earth., 25(1), 17-24, doi:10.1016/S1464-1895(00)00004-1, 2000.

Andersen, O. B., Knudsen, P., and Stenseng, L.: The DTU13 global mean sea surface from 20 years of satellite altimetry, In: OSTST Meeting, Boulder, Colo, 2013.

Artemieva, I.M. and Thybo, H.: EUNAseis: A seismic model for Moho and crustal structure in Europe, Greenland, and the North Atlantic region, Tectonophysics, 609, 97-153, doi:10.1016/j.tecto.2013.08.004, 2013.

Audet, P.: Toward mapping the effective elastic thickness of planetary lithospheres from a spherical wavelet analysis of gravity and topography, Phys. Earth. Planet. In., 226(1), 48-82, doi: 10.1016/j.pepi.2013.09.011, 2014.

Becker, S., Brockmann, J. M., and Schuh, W. D.: Mean dynamic topography estimates purely based on GOCE gravity field models and altimetry, Geophys. Res. Lett., 41, 2063-2069, doi:10.1002/2014GL059510, 2014.

Bentel, K., Schmidt, M. and Rolstad, D.C.: Artifacts in regional gravity representations with spherical radial basis functions, Journal of Geodetic Science, 3(3), 173-187, doi:10.2478/jogs-2013-0029, 2013.

Bingham, R. J., Haines, K., and Lea, D. J.: How well can we measure the ocean's mean dynamic topography from space? J. Geophys. Res. Oceans, 119, 3336-3356, doi: 10.1002/2013JC009354, 2014.

Blundell, D.J., Hobbs, R.W., Klemperer, S.L., Scott-Robinson, R., Long, R.E., West, T.E. and Duin, E.: Crustal structure of the central and southern North Sea from BIRPS deep seismic reflection profiling, Journal of the Geological Society, 148, 445-457, 1991.

Burnham, K. P., Anderson, D. R.: Model Selection and Multimodel Inference: A practical information-theoretic approach (2nd ed.), Springer-Verlag, ISBN 0-387-95364-7, 2002.

Chambodut, A., Panet, I., Mandea, M., Diament, M., Holschneider, M. and Jamet, O.: Wavelet frames: an alternative to spherical harmonic representation of potential fields, Geophys. J. Int., 163(3), 875-899, doi:10.1111/j.1365-246X.2005.02754.x, 2005.

Cianciara, B. and Marcak, H.: Interpretation of gravity anomalies by means of local power spectra, Geophys. Prospect., 24 (2), 273-286, doi: 10.1111/j.1365-2478.1976.tb00925.x, 1976.

Denker, H.: Regional Gravity Field Modeling: Theory and Practical Results, In: G Xu (ed)Sciences of 641 Geodesy - II, 185-291, Springer, Berlin, Heidelberg, 2013.

Eicker, A., Schall, J. and Kusche, J.: Regional gravity modeling from spaceborne data: case studies with GOCE, Geophys. J. Int., 196(3), 1431-1440, doi:10.1093/gji/ggt485, 2013.

Fengler, M.J., Freeden, W., Kohlhaas, A., Michel, V. and Peters, T.: Wavelet Modeling of Regional and Temporal Variations of the Earth's Gravitational Potential Observed by GRACE, J. Geod., 81(1), 5-15, doi: 10.1007/s00190-006-0040-1, 2007.

Fengler, M.J., Freeden, W. and Michel, V.: The Kaiserslautern multiscale geopotential model SWITCH-03 from orbit perturbations of the satellite CHAMP and its comparison to the models EGM96, UCPH2002_02_0.5, EIGEN-1s and EIGEN-2, Geophys. J. Int., 157(2), 499-514, doi:10.1111/j.1365-246X.2004.02209.x, 2004.

Fichler, C. and Hospers, J.: Deep crustal structure of the northern North Sea Viking Graben: results from deep reflection seismic and gravity data, Tectonophysics, 178, 241-254, 1990.

Forsberg, R. and Tscherning, C.C.: An overview manual for the GRAVSOFT geodetic gravity field modeling programs, 2nd edn. National Space Institute, Denmark and Niels Bohr Institute, University of Copenhagen, 2008.

Förste, C., Bruinsma, S.L., Abrikosov, O., Lemoine, J.M., Schaller, T., Götze, H.J., Ebbing, J., Marty, J.C., Flechtner, F., Balmino, G. and Biancale, R.: EIGEN-6C4 The latest combined global gravity field model including GOCE data up to degree and order 2190 of GFZ Potsdam and GRGS Toulouse. The 5th GOCE User Workshop, Paris, France, 2014.

Fotopoulos, G.: Calibration of geoid error models via a combined adjustment of ellipsoidal, orthometric and gravimetric geoid height data. J. Geod., 79(1),111-123, doi:10.1007/s00190-005-0449-y, 2005.

Freeden, W., Gervens, T. and Schreiner, M.: Constructive Approximation on the Sphere (With Applications to Geomathematics). Oxford Sci. Publ., Clarendon Press, Oxford, 1998.

Freeden, W., Fehlinger, T., Klug, M., Mathar, D. and Wolf, K.: Classical globally reflected gravity field determination in modern locally oriented multiscale framework. J. Geod., 83, 1171-1191, doi:10.1007/s00190-009-0335-0, 2009.

Freeden, W. and Schreiner, M.: Local multiscale modelling of geoid undulations from deflections of the vertical, J. Geod., 79, 641-651, doi: 10.1007/s00190-005-0017-5, 2006.

Gilardoni, M., Reguzzoni, M., Sampietro, D.: GECO: a global gravity model by locally combining GOCE data and EGM2008, Studia Geophysica et Geodaetica, 60 (2), 228-247, doi:10.1007/s11200-015-1114-14, 2015.

Grad, M. and Tiira, T.: TheMoho depthmap of the European Plate. Geophys. J. Int., 176, 279-292, doi:10.1111/j.1365-246X.2008.03919.x, 2009.

Gruber, T., Rummel, R., Abrikosov, O., and van Hees, R.: GOCE Level 2 Product Data Handbook. GO-MA-HPF-GS-0110, Issue 4.2. (http://earth.esa.int/pub/ESA_DOC/GOCE/GOMA-HPF-GS-0110_4.2-ProductDataHandbook.pdf), 2010.

Hipkin, R.G., Haines, K., Beggan, C., Bingley, R., Hernandez, F., Holt, J. and Baker, T.: The geoid EDIN2000 and mean sea surface topography around the British Isles, Geophys. J. Int., 157(2), 565-577, doi:10.1111/j.1365-246X.2004.01989.x, 2004.

Holschneider, M. and Iglewska-Nowak, I.: Poisson wavelets on the sphere. J. Fourier. Anal. Appl., 13(4), 405-419, doi:10.1007/s00041-006-6909-9, 2007.

Idžanović, M., Ophaug, V., and Andersen, O. B.: The coastal mean dynamic topography in Norway observed by CryoSat-2 and GOCE, Geophys. Res. Lett., 44, 5609-5617, doi:10.1002/ 2017GL073777, 2017.

Jiang, W., Zhang, J., Tian, T. and Wang, X.: Crustal structure of Chuan-Dian region derived from gravity data and its tectonic implications, Phys. Earth. Planet. Interiors., 212-213, 76-87, doi: 10.1016/j.pepi.2012.07.001, 2012.

Klees, R., Prutkin, I.: The combination of GNSS-levelling data and gravimetric (quasi-) geoid heights in the presence of noise. J. Geod., 84(12), 731-749, doi:10.1007/s00190-010-0406-2, 2008.

Klees, R., Tenzer, R., Prutkin, I. and Wittwer, T.: A data-driven approach to local gravity field modelling using spherical radial basis functions, J. Geod., 82(8), 457-471, doi:10.1007/s00190-007-0196-3, 2008.

Koch, K.R. and Kusche, J.: Regularization of geopotential determination from satellite data by variance components, J. Geod., 76, 259-268, doi: 10.1007/s00190-002-0245-x, 2002.

Kusche, J.: A Monte-Carlo technique for weight estimation in satellite geodesy, J. Geod., 76(11), 641-652, doi:10.1007/s00190-002-0302-5, 2003.

Liang, W., Xu, X., Li, J. and Zhu, G.: The determination of an ultra high gravity field model SGG-UGM-1 by combining EGM2008 gravity anomaly and GOCE observation data, Acta Geodaeticaet Cartographica Sinica, 47(4), 425-434, doi:10.11947/j.AGCS.2018.20170269, 2018.

Lieb, V., Schmidt, M., Dettmering, D. and Börger, K.: Combination of various observation techniques for regional modeling of the gravity field, J. Geophys. Res. Solid Earth, 121, 3825-3845, doi:10.1002/2015JB012586, 2016.

Mayer-Gürr, T., Pail, R., Gruber, T., Fecher, T., Rexer, M., Schuh, W.-D., Kusche, J., Brockmann, J.-M., Rieser, D., Zehentner, N., Kvas, A., Klinger, B., Baur, O., Höck, E., Krauss, S., and Jäggi, A.: The combined satellite gravity field model GOCO05s, Geophys Res Abs 17:EGU2015-12364, 2015.

Naeimi, M., Flury, J. and Brieden, P.: On the regularization of regional gravity field solutions in spherical radial base

functions, Geophys. J. Int., 202, 1041-1053, doi:10.1093/gji/ggv210, 2015.

Nahavandchi, N., Soltanpour, A.: Improved determination of heights using a conversion surface by combining gravimetric quasi-geoid/geoid and GNSS-levelling height differences. Stud. Geophys. Geod., 50(2), 165-180, doi:10.1007/s11200-006-0010-3, 2006.

Omang, O.C.D. and Forsberg, R.: How to handle topography in practical geoid determination: three examples, J. Geod., 74(6), 458-466, doi:10.1007/s001900000107, 2000.

Panet, I., Kuroishi, Y. and Holschneider, M.: Wavelet modelling of the gravity field by domain decomposition methods: an example over Japan, Geophys. J. Int., 184(1), 203-219, doi:10.1111/j.1365-246X.2010.04840.x, 2011.

Pavlis, N.K., Holmes, S.A., Kenyon, S.C. and Factor, J.F.: The development and evaluation of Earth Gravitational Model (EGM2008), J. Geophys. Res., 117, B04406, doi:10.1029/2011JB008916, 2012.

Prutkin, I., Klees, R.: On the non-uniqueness of local quasi-geoids computed from terrestrial gravity anomalies. J. Geod., 82(3), 147-156, doi:10.1007/s00190-007-0161-1, 2008.

Rummel, R., Balmino, G., Johannessen, J., Visser, P., and Woodworth, P.: Dedicated gravity field missions-Principle and aims, J. Geodyn., 33(1), 3-20, doi:10.1016/S0264-3707(01)00050-3, 2002.

Schmidt, M., Fengler, M., Mayer-Gürr, T., Eicker, A., Kusche, J., Sánchez, L. and Han, S.C.: Regional gravity modeling in terms of sphericalbase functions, J. Geod., 81(1), 17-38, doi:10.1007/s00190-006-0101-5, 2007.

Schmidt, M., Fabert, O., Shum, C.K.: On the estimation of a multi-resolution representation of the gravity field based on spherical harmonics and wavelets, J. Geodyn., 39(1), 512-526, doi: 10.1016/j.jog.2005.04.007, 2005.

Schmidt, M., Han, S.C., Kusche, J., Sanchez, L. and Shum, C.K.: Regional high- resolution spatiotemporal gravity modeling from GRACE data using spherical wavelets, Geophys. Res. Lett., 33, L08403, doi:10.1029/2005GL025509, 2006.

Sjöberg, L. E.: A discussion on the approximations made in the practical implementation of the remove-compute-restore technique in regional geoid modelling, J. Geod., 78, 645-653, doi:10.1007/s00190-004-0430-1, 2005.

Slobbe, D. C.: Roadmap to a mutually consistent set of offshore vertical reference frames, PhD thesis, The Netherland, 2013.

Slobbe, D.C., Klees, R. and Gunter, B.C.: Realization of a consistent set of vertical reference surfaces in coastal areas, J. Geod., 88(6), 601-615, doi:10.1007/s00190-014-0709-9, 2014.

Spector, A. and Grant, F.S.: Statistical models for interpreting aeromagnetic data, Geophysics, 35(2), 293-302,

doi:10.1190/1.1440092, 1970.

Syberg, F.J.R.: A Fourier method for the regional-residual problem of potential fields, Geophys. Prospect., 20 (1), 47-75, doi:10.1111/j.1365-2478.1972.tb00619.x, 1972.

Tapley, B. D., Bettadpur, S., Watkins, M. and Reigber, C.: The gravity recovery and climate experiment: Mission overview and early results, Geophys. Res. Lett., 31, L09607, doi:10.1029/2004GL019920, 2004.

Tenzer, R. and Klees, R.: The choice of the spherical radial basis functions in local gravity field modeling. Stud. Geophys. Geod., 52(3), 287-304, doi:10.1007/s11200-008-0022-2, 2008.

Tenzer, R., Klees, R. and Wittwer, T.: Local Gravity Field Modelling in Rugged Terrain Using Spherical Radial Basis Functions: Case Study for the Canadian Rocky Mountains. In S. Kenyon, Geodesy for Planet Earth, International Association of Geodesy Symposia 136, Springer-Verlag Berlin Heidelberg, pp 401-409, 2012.

Tscherning, C.C.: Introduction to functional analysis with a view to its application in approximation theory. In: Moritz H, Sünkel H(eds)Approximation methods in geodesy, Karlsruhe, Germany, 1978.

Wang, Y., Saleh, J., Li, X., and Roman, D. R.: The US Gravimetric Geoid of 2009 (USGG2009): model development and evaluation, J. Geod., 86(3), 165-180, doi:10.1007/s00190-011-0506-7, 2012.

Wittwer, T.: Regional gravity field modelling with radial basis functions, Dissertation, Delft University of Technology, Delft, The Netherlands, 2009.

Wu, Y., Luo, Z., Chen, W. and Chen, Y.: High-resolution regional gravity field recovery from Poisson wavelets using heterogeneous observational techniques, Earth Planets Space, 69:34, doi:10.1186/s40623-017-0618-2, 2017a.

Wu, Y., Luo, Z. and Zhou, B.: Regional gravity modelling based on heterogeneous data sets by using Poisson wavelets radial basis functions, Chin. J. Geophys (in Chinese), 59(3):852-864, doi:10.6038/cjg20160308, 2016.

Wu, Y., Zhong, B., Luo, Z.: Investigation of the Tikhonov regularization method in regional gravity field modeling by Poisson wavelets radial basis functions, Journal of Earth Science,9,1-10, doi: 10.1007/s12583-017-0771-32016, 2017b.

Wu, Y., Zhou, H., Zhong, B., and Luo, Z.: Regional gravity field recovery using the GOCE gravity gradient tensor and heterogeneous gravimetry and altimetry data, J. Geophys. Res. Solid Earth, 122(8), 6928-6952, doi: 10.1002/2017JB014196, 2017c.

Xu, C., Liu, Z., Luo, Z., Wu, Y. and Wang, H.: Moho topography of the Tibetan Plateau using multi-scale gravity analysis and its tectonic implications, J. Asian. Earth. Sci., 138, 378-386, doi: 10.1016/j.jseaes.2017.02.028, 2017.

Xu, C., Luo, Z., Sun, R., Zhou, H., Wu, Y.: Multilayer densities using a wavelet-based gravity method and their tectonic implications beneath the Tibetan Plateau, Geophys. J. Int., 213, 2085-2095, doi: 10.1093/gji/ggy110, 2018.

Ziegler, P.A. and Dèzes, P.: Crustal evolution of western and central Europe, European Lithosphere Dynamics, In: Gee, D., Stephenson, R. (Eds.), Geol. Soc. London Sp. Publ., 32, 43-56, 2006.